THE UNIVERSITY OF MICHIGAN

INDUSTRY PROGRAM OF THE COLLEGE OF ENGINEERING

EFFECT OF VARIATION OF ACCELERATION ON FREE-SURFACE INSTABILITY

Chia-Shun Yih
S. P. Lin

April, 1963

IP-614

LIST OF CONTENTS

LIST OF FIGURES AND PLATES

1. INTRODUCTION

The instability of stock on a Fourdrinier wire occurs as it issues from the slice, as it passes over the table rolls, and especially immediately after it leaves the table rolls. There are many causes for the instability. On top of the table rolls the cause of instability is the centripetal and downward acceleration of the fluid, which can be many times as great as the gravitational acceleration. A paper dealing with this was published in the Proceedings of the Royal Society by Yih[1,2] with supporting experimental data. At the places where the streamlines are curved and the fluid is slowed down away from the center of the curvature, instability may take the form of the formation of Taylor-Görtler vortices. A paper dealing with this possibility was published by Yih and Debler in 1961.[2]

Measurements of the growth of disturbances after the table roll were made by Spengos,[3] who also obtained some preliminary measurements on the rate of growth of the disturbances over the table roll. But the rather violent instability of the stock after the table rolls has so far not been satisfactorily explained. This paper provides a theory, with some supporting experimental data, which explains the main cause of instability after the table rolls, and constitutes a final report to the Technical Association of Pulp and Paper Industries which has generously sponsored the study of free-surface instability at the University of Michigan during the years 1957-59 and 1960-62.

2. A DESCRIPTIVE EXPLANATION OF THE CAUSE OF POST-ROLL INSTABILITY

Consider a layer of liquid in a container and in wave motion, as shown in Figure 1. Suppose that at time $t = 0$ the wave attains a maximum height, when the acceleration of the container is a_1, directed upward. This acceleration is maintained until the free surface is flat, at which time all the energy of the wave motion is in the form of kinetic energy. If at this time the acceleration is suddenly changed to a_2, which is less than a_1, then as the next maximum wave height is attained it would have to be greater than the previous maximum, because the potential energy relative to the container will remain the same, whereas the effective gravitational acceleration has been decreased from $g + a_1$ to $g + a_2$. The reverse is true if a_2 is greater than a_1, as shown in Figure 2. It is also evident that the phase of the waves is important at the moment of change of the acceleration, whether it is decreased or increased. Since the waves on the stock as it moves past the table rolls are in all possible phases, a change of acceleration will make certain components of the waves unstable. The change of acceleration is experienced by the stock as the wire carrying it leaves the table rolls, above which it has undergone a downward acceleration, and goes through a region of reverse curvature, in which it is subjected to an upward acceleration. The first author owes this idea to a stimulating discussion with Mr. J.T. Justus, who explained the instability in terms of pressure at the bottom of the container. A more precise explanation will be given by a mathematical analysis, which will be presented in the following two sections.

The foregoing consideration of the instability phenomenon, for the first time, also explains in physical terms the observation of Faraday in 1831 (Phil. Trans., p. 319) that the frequency of liquid oscillations was only half that of an oscillating vessel containing the liquid, since, as the liquid accomplishes half an oscillation (Figure 1), the vessel has already accomplished one oscillation, ready to start the next cycle by changing a_2 to a_1 again. (The change in acceleration occurs both at extreme wave heights and at zero wave heights.)

3. FORMULATION OF THE DIFFERENTIAL EQUATION GOVERNING FREE-SURFACE INSTABILITY

Wave motion in a layer of liquid of uniform depth will be considered. The formulation of the problem is identical to that of Benjamin and Ursell[5] for instability due to periodic acceleration. In fact, the qualitative explanation given in the previous section makes it possible to understand in physical terms the mathematical results obtained by Benjamin and Ursell.

The hydrodynamic equations of motion with reference to the container are, with viscous effects neglected,

$$\frac{D}{Dt}(u,v,w) = \frac{1}{\rho}\left(\frac{\partial}{\partial x}, \frac{\partial}{\partial y}, \frac{\partial}{\partial z}\right) p + (0,0, -g-a), \qquad (1)$$

in which a is the acceleration, ρ is the density, p is the pressure, g is the gravitational acceleration, and u, v, and w are the velocity components in the directions of increasing x, y, and z respectively. The coordinates x, y, and z are Cartesian coordinates, and the symbol $\frac{D}{Dt}$ stands for

$$\frac{\partial}{\partial t} + u\frac{\partial}{\partial x} + v\frac{\partial}{\partial y} + w\frac{\partial}{\partial z},$$

and is the operator for substantial differentiation. From Equation (1), it can already be seen that when the frame of reference is taken to be the container, the body force g per unit mass in the negative z-direction is replaced by $g + a$, so that the potential energy with respect to the container is based on $g + a$ instead of g. Although the concept of potential energy is meaningful only if a is constant, the explanation based

on constant a given in the last section is qualitatively applicable to the case of variable acceleration.

The unknowns in (1) are u, v, w, and p. Since there are only three equations in (1), a fourth one is needed. This is the equation of continuity

$$\frac{\partial u}{\partial x} + \frac{\partial v}{\partial y} + \frac{\partial w}{\partial z} = 0 \ . \tag{2}$$

Now Equations (1) are nonlinear, and are very difficult to solve although the number of equations is now sufficient with the addition of (2). Fortunately, the theorem of Helmholtz and Kelvin on the persistence of irrotationality is valid here because the acceleration a of the container can only be time-dependent, so that the effective body force with components (0, 0, -g-a) is conservative, i.e., its curl is zero. This can be demonstrated quite simply. With the vorticity components denoted by

$$\xi = \frac{\partial w}{\partial y} - \frac{\partial v}{\partial z}, \quad \eta = \frac{\partial u}{\partial z} - \frac{\partial w}{\partial x}, \quad \zeta = \frac{\partial v}{\partial x} - \frac{\partial u}{\partial y}, \tag{3}$$

equations governing the vorticity of the fluid can be obtained from (1) by cross-differentiation. For instance, with the second and third equation in (1) written as

$$\frac{\partial v}{\partial t} + u\zeta - w\xi = - \frac{\partial}{\partial y}\left(\frac{p}{\rho} + \frac{u^2+v^2+w^2}{2}\right) \ , \tag{4}$$

$$\frac{\partial w}{\partial t} - u\eta + v\xi = - \frac{\partial}{\partial z}\left(\frac{p}{\rho} + \frac{u^2+v^2+w^2}{2}\right) - (g+a), \tag{5}$$

(5) can be differentiated with respect to y and (4) differentiated with respect to z. Utilizing (2) and the identity

$$\frac{\partial \xi}{\partial x} + \frac{\partial \eta}{\partial y} + \frac{\partial \zeta}{\partial z} = 0 \ ,$$

the result can be reduced to the form

$$\frac{D\xi}{Dt} = \xi \frac{\partial u}{\partial x} + \eta \frac{\partial u}{\partial y} + \zeta \frac{\partial u}{\partial z} . \tag{6}$$

Similarly,

$$\frac{D\eta}{Dt} = \xi \frac{\partial v}{\partial x} + \eta \frac{\partial v}{\partial y} + \zeta \frac{\partial v}{\partial z} , \tag{7}$$

$$\frac{D\zeta}{Dt} = \xi \frac{\partial w}{\partial x} + \eta \frac{\partial w}{\partial y} + \zeta \frac{\partial w}{\partial z} . \tag{8}$$

Now if the flow starts from an irrotational state, $\xi = \eta = \zeta = 0$ everywhere at $t = 0$. Then (6), (7), and (8) state that the substantial derivatives of ξ, η, and ζ are zero, or that the true derivatives of ξ, η, and ζ of each particle as we follow its motion are zero. This being ture of every particle originating from an irrotational state, the vorticity of every particle will remain zero, and the persistence of irrotationality is demonstrated. Since the motion under consideration can be considered to have started from rest, which is an irrotational state, the subsequent motion is irrotational.

For irrotational motion, Equation (3) states that the curl of the velocity is zero. This implies that the velocity can be expressed as the gradient of a potential ϕ :

$$(u,v,w) = - \left(\frac{\partial}{\partial x}, \frac{\partial}{\partial y}, \frac{\partial}{\partial z}\right) \phi , \tag{9}$$

Combining (2) and (9), we have

$$\left(\frac{\partial^2}{\partial x^2} + \frac{\partial^2}{\partial y^2} + \frac{\partial^2}{\partial z^2}\right) \phi = 0 , \tag{10}$$

which is linear. The problem is then to solve (10) with the appropriate boundary conditions. But one of the boundary conditions, the one at the free surface, involves the pressure. It is therefore necessary to obtain an expression for p in terms of ϕ. This is supplied by the Bernoulli equation for irrotational unsteady flows:

$$-\frac{\partial\phi}{\partial t} + \frac{p}{\rho} + \frac{u^2+v^2+w^2}{2} + (g+a)z = F(t) \ . \qquad (11)$$

The derivation of (11) is quite simple. With the vorticity components in (4) and (5) equal to zero, and with v and w on the left-hand sides given by (9), the Equations (4) and (5) can be written as

$$\frac{\partial\chi}{\partial y} = 0, \quad \frac{\partial\chi}{\partial z} = 0 \ ,$$

in which

$$\chi = -\frac{\partial\phi}{\partial t} + \frac{p}{\rho} + \frac{u^2+v^2+w^2}{2} + (g+a)\ z \ .$$

Similarly the first equation in (1) gives

$$\frac{d\chi}{dx} = 0 \ .$$

Hence, by integration, (11) is obtained. The function $F(t)$ is independent of x, y, and z, and can be absorbed in ϕ by adding to ϕ the function $-\int F(t)dt$, without affecting either the velocity components or p. Hence, for convenience $F(t)$ will be taken to be zero.

The conditions at the rigid boundaries are

$$\frac{\partial\phi}{\partial z} = 0 \quad \text{at the bottom,} \qquad (12)$$

and

$$\frac{\partial\phi}{\partial n} = 0 \quad \text{at the walls.} \qquad (13)$$

At the free surface,

$$p = T\left(\frac{1}{R_1} + \frac{1}{R_2}\right) , \tag{14}$$

in which T is the surface tension and R_1 and R_2 are the principal radii of the surface

$$z = \zeta(x,y,t) , \tag{15}$$

with ζ now and henceforth denoting the surface displacement rather than the third vorticity component. Since (15) is valid for all values of time t,

$$\frac{D}{Dt}[z - \zeta(x,y,t)] = 0 ,$$

or

$$w = \frac{\partial \zeta}{\partial t} + u \frac{\partial \zeta}{\partial x} + v \frac{\partial \zeta}{\partial y} . \tag{16}$$

This is the kinematic condition at the free surface, relating w to ζ. The dynamic boundary condition is obtained from (11) and (14), and is

$$\frac{T}{\rho}\left(\frac{1}{R_1} + \frac{1}{R_2}\right) - \frac{\partial \phi}{\partial t} + \frac{1}{2}(u^2+v^2+w^2) + (g+a)\zeta = 0 . \tag{17}$$

If ζ and its derivatives with respect the x and y are everywhere small, u, v, and w will be everywhere small, and squares and products in u, v, w, and ζ can be neglected. Equations (16) and (17) can then be written as

$$w = \frac{\partial \zeta}{\partial t} = \frac{\partial \phi}{\partial z} \quad \text{at} \quad z = h, \tag{18}$$

$$\frac{T}{\rho}\left(\frac{\partial^2 \zeta}{\partial x^2} + \frac{\partial^2 \zeta}{\partial y^2}\right) - \left.\frac{\partial \phi}{\partial t}\right|_{z=h} + (g+a)\zeta = 0 . \tag{19}$$

Following Benjamin and Ursell,[5] we shall take

$$\zeta(x,y,t) = \sum_{0}^{\infty} a_m(t) S_m(x,y) \ , \tag{20}$$

and

$$\phi(x,y,z,t) = \sum_{1}^{\infty} \frac{da_m(t)}{dt} \frac{\cosh k_m\zeta}{k_m \sinh k_m h} S_m(x,y) + G(t) \ , \tag{21}$$

in which $S_m(x,y)$ satisfies

$$\left(\frac{\partial^2}{\partial x^2} + \frac{\partial^2}{\partial y^2} + k_m^2\right) S_m(x,y) = 0 \ , \tag{22}$$

in which the k's are the eigenvalues that make $\frac{\partial S_m(x,y)}{\partial n}$ equal to zero, and of course depend only on the shape of the container. Note that (13) and (18) imply that

$$\frac{\partial \zeta}{\partial n} = 0 \quad \text{at the walls,}$$

and that Equation (20) satisfies this condition. Also, ϕ given in (21) satisfies (12) and (13), as well as (18).

The eigenvalue $k_o = 0$ corresponds to $S_o(x,y) = 0$. As explained by Benjamin and Ursell, $a_o(t)$ is constant, since the total volume of the liquid is constant. If the origin of ζ is taken from the mean free surface, $a_o(t) = 0$. Hence, it follows from (19) that $G(t)$ can only be a constant, which can be taken to be zero without affecting anything. With (20) and (21) substituted into (19), the result is

$$\sum_{1}^{\infty} \frac{S_m(x,y)}{k_m \tanh k_m h} \left[\frac{d^2 a_m}{dt^2} + k_m \tanh k_m h \left(\frac{k_m^2 T}{\rho} + g + a\right)\right] = 0 \ . \tag{23}$$

Since the functions $S_m(x,y)$ are linearly independent,

$$\frac{d^2 a_m}{dt^2} + (p_m + q_m)\, a_m = 0 \ , \tag{24}$$

in which

$$p_m = k_m \tanh k_m h\left(\frac{T}{\rho} k_m^2 + g\right), \quad q_m = a(t)\, k_m \tanh k_m h. \tag{25}$$

Equation (24) is the basis for the analyses in the subsequent sections.

4. FREE-SURFACE INSTABILITY DUE TO A SUDDEN CHANGE OF ACCELERATION

To bring out the effect of variable acceleration on the amplitude of waves, consider the simplest case in which the acceleration is zero at first, then assumes a constant finite value a, and finally becomes zero again, as shown in Figure 3.

For simplicity the quantity a_m, which is a time-dependent amplitude in the sense that it is proportional to the maximum surface height (with respect to x and y) at time t for the m-th mode, will be denoted by A. If attention is focused on the m-th mode, (24) reads

$$\frac{d^2A}{dt^2} + (p_m+q_m)A = 0 \ . \tag{26}$$

Suppose that the acceleration $a(t)$ is changed from zero to the constant a at time $t = 0$. Then for $t < 0$,

$$A = B_1 \cos(s_1 t + \Theta_1) \ , \qquad B_1 > 0 \ . \tag{27}$$

in which $s_1^2 = p_m$, and Θ_1 is the angle specifying the phase of A at $t = 0$. For $t > 0$ the acceleration is a, so that the solution of (26) is

$$A = B_2 \cos(s_2 t + \Theta_2) \ , \tag{28}$$

in which

$$s_2^2 = p_m+q_m \ , \qquad \text{with} \quad a(t) = a \quad \text{in} \quad q_m \ .$$

Now at $t = 0$ both A and $\frac{dA}{dt}$ must be continuous. Hence

$$B_1 \cos\Theta_1 = B_2 \cos\Theta_2 \ , \tag{29}$$

$$s_1 B_1 \sin\Theta_1 = s_2 B_2 \sin\Theta_2 \ . \tag{30}$$

If (29) is squared and (30) is divided by s_2 and squared, and the results are added, the following equation is obtained:

$$B_2^2 = B_1^2[\cos^2\theta_1 + (\frac{s_1}{s_2}\sin\theta_1)^2] = B_1^2[1 - (1-r^2)\sin^2\theta_1] \ , \quad (31)$$

in which

$$r = \frac{s_1}{s_2} \ .$$

Thus, whatever the value of r, $|B_2| = |B_1|$ if $\theta_1 = 0$. That is to say, the amplitude is unchanged if the change of acceleration from zero to a occurs at the time of maximum A. This is understandable, because at that moment the kinetic energy is zero, and a sudden change in acceleration only brings about a sudden change in potential energy in the proportion $(g+a)/g$. If the acceleration is maintained constant ($= a$), the subsequent maximum A will remain unchanged.

If, on the other hand, $\theta_1 = \pi/2$, then

$$|B_2| = r|B_1| \ , \quad (32)$$

and the amplitude is reduced by the ratio r. We can, indeed, compute the maximum and minimum of $(B_2/B_1)^2$ from (31). Thus

$$\frac{d}{d\theta_1}(\frac{B_2}{B_1})^2 = -2(1-r^2)\sin\theta_1\cos\theta_1 = -(1-r^2)\sin 2\theta_1 \ ,$$

which is zero for $\theta_1 = 0, \pm\pi/2, \pm\pi, \pm 3\pi/2$, etc. Since $r < 1$, it is easy to see that the values 0, and $\pm n\pi$ (n = integer) correspond to the maximum values of $|B_2/B_1|$, and the values $\pm(2n+1)\pi/2$ correspond to the minimum values. In other words, the most severe amplitude-reduction ratio is simply s_1/s_2.

When the acceleration suddenly drops from a to zero, the analysis is similar, but physically the situation is quite different. Since we are going to consider all possible phase angles, we can again take, without loss of generality, the moment of acceleration change to be the origin of time. For $t < 0$, we have

$$A = B_2 \cos(s_2 t + \theta_2') , \tag{33}$$

in which s_2 is as defined before, $|B_2|$ maintains the same magnitude, but θ_2' is no longer θ_2, because we have changed the origin of time for convenience. For $t > 0$,

$$A = B_3 \cos(s_1 t + \theta_3) , \tag{34}$$

in which $s_1 = \sqrt{p_m}$ as before. Continuity in A and $\frac{dA}{dt}$ at $t = 0$ demands that

$$B_2 \cos\theta_2' = B_3 \cos\theta_3 ,$$
$$s_2 B_2 \sin\theta_2' = s_1 B_3 \sin\theta_3 ,$$

which produce

$$B_3^2 = B_2^2[1 + (r^{-2}-1) \sin^2\theta_2'] , \tag{35}$$

in which r has the same meaning as before. A similar calculation gives the maximum value for $|B_3/B_2|$ to be r^{-1}, and the minimum value to be 1. The minimum value, corresponding to no change of amplitude, is again understandable. Since it corresponds to $\theta_2' = 0$ or $n\pi$, it corresponds to the state of maximum potential energy and no kinetic energy.

The maximum value of $|B_3/B_2|$ correspond to $\Theta_2' = \frac{\pi}{2}$ or $\pm(2n+1)\pi/2$. For $0 < \Theta_2' < \pi/2$, the value of $|B_3/B_2|$ is between 1 and $1/r$. This brings out the importance of the phase angle Θ_2'. (The same is true of Θ_1.) Since waves with all phases are assumed to exist, the maximum ratio of amplitude increase is s_2/s_1.

Consider now the acceleration graph given in Figure 3. If $t_o = 0$ and $\Theta_1 = 0$, the amplitude suffers no change on passing through t_o. At $t = t_1$ the value of Θ_2' is really $s_2(t_1-t_o) + \Theta_2 = s_2t_1 + \Theta_2$. Depending on s_1, s_2, and t_1 (or t_1-t_o), it may or may not be one of the values $\pm (2n+1)\pi/2$. But as t_1 is varied, it can be one of these values. Thus the absolute maximum for $|B_3/B_1|$, or the greatest ratio of amplitude increase, is s_2/s_1. If the value a is very large, say 48 g, this ratio is exactly 7 if surface-tension effect is neglected, because $(a+g)/g = 7^2$. It is significant that it is the region of acceleration decrease that causes the increase in amplitude. At the post-roll region on a Fourdrinier wire, the velocity changes from a downward one along the roll to a slightly upward one along the wire a short distance after a reverse curvature (concave upward), then becomes horizontal again. There is a region where the acceleration changes from a large positive value (upward acceleration) to zero. This is the narrow region of dramatic increase in the amplitudes of the disturbances.

The acceleration schedule described by Figure 4 is more realistic. The downward acceleration a_1 corresponds to the region over the table roll. The upward acceleration, a, corresponds to the region of reverse curvature (concave upward). But the wire has to become horizontal

finally. So there must be a region of upward convexity again, corresponding to downward acceleration a_2. At $t = t_o$ the greatest amplitude ratio is 1, whatever the values of a_1 and a. At $t = t_1$ the maximum possible amplitude ratio is

$$\left(\frac{g+a}{g-a_2}\right)^{1/2},$$

which is also the maximum ratio of the amplitude after t_2 to the amplitude before t_1. Since a_2 may be quite near to g, this ratio can be very large. This explains the rather dramatic amplification of disturbances in the post-roll region.

5. FREE-SURFACE INSTABILITY DUE TO A GRADUAL CHANGE OF ACCELERATION

An acceleration schedule representing the actual situation on a Fourdrinier wire is given in Figure 5. The region $t < t_o$ represents the region of downward acceleration over the table rolls. The region $t_o \leq t \leq t_1$ represents the region of increasing upward acceleration. The region $t_1 \leq t \leq t_2$ represents the region of decreasing acceleration. For $t > t_2$, a region of negative (downward) accelera- again exists, which corresponds to a region of upward-convexity of the Fourdrinier wire, following the region of reverse curvature (concave upward) where the acceleration is positive.

The governing equation is still (26), in which p_m and q_m retain their forms in (25), so that

$$\frac{q_m}{k_m \tanh k_m h} = a(t) = \begin{cases} -a_o \quad \text{for} \quad t \leq t_o \ , \\ a_o + \dfrac{a_1+a_o}{t_1-t_o}(t-t_o) \quad \text{for} \quad t_o \leq t \leq t_1, \\ a_1 - \dfrac{a_1+a_2}{t_2-t_1}(t-t_1) \quad \text{for} \quad t_1 \leq t \leq t_2, \\ -a_2 \quad \text{for} \quad t \geq t_2 \ . \end{cases}$$

Thus it is easy to see that (26) has in all four regions the general form

$$\frac{d^2A}{dt^2} + (\alpha + \beta t)A = 0 \ . \tag{36}$$

If β is zero, as for $t \leq t_o$ or $t \geq t_2$, then the solution is of the form

$$A = B \cos (\sqrt{\alpha}\, t + \theta) \ . \tag{37}$$

If β is not zero, as in the region of increasing or decreasing acceleration, the solution of (36) is

$$A = (\alpha+\beta t)^{1/2}[B\, J_{1/3}(\tfrac{2}{3}\sqrt{\beta}(t + \tfrac{\alpha}{\beta})^{3/2}) + N_{1/3}(\tfrac{2}{3}\sqrt{\beta}(t + \tfrac{\alpha}{\beta})^{3/2})] \quad . \quad (38)$$

Matching of the solutions of types (37) and (38) at $t = t_o$ and $t = t_2$, and of two solutions of the type (38) at $t = t_1$, can be made on the demand that A and dA/dt be continuous at the moments t_o, t_1, and t_2. Since the possibility of tremendous increase in amplitude has already been demonstrated in the last section for acceleration schedules described by Figures 3 and 4, and the demonstration for the present case would differ only in some detail, it will not be given here. Instead, (37) and (38) will be used to correlate the experimental data, because the actual acceleration schedule in the experiments is not far from that given in Figure 5.

6. EXPERIMENTAL VERIFICATION

The theory has been advanced that variable acceleration in a direction normal to the free surface can bring about a tremendous increase in amplitude of surface disturbances. To test the validity of this theory, an apparatus was constructed (See Plate I) which allowed a plastic 5-inch-square box containing a layer of water to fall about 2 to 3 inches onto a pad of foam-rubber layers. Surface disturbances were made by either one line-jet of air blowing at the middle of the water surface or two such jets parallel to two sides of the box and blowing at two symmetric quarter positions (hence not at the center line). Thus the wave lengths were controlled. When only one jet was used, the wave length λ is equal to the inner measure of the side of the box (5 inches). When two jets were used, the wave length was one half of that.

As the water-bearing box was released, it fell with very nearly the downward acceleration g. When it hit the pad, this acceleration was first reduced to zero, then became positive, reaching a large positive value after some fluctuations, then decreased to a downward acceleration a_2, say, for a length of time before finally becoming zero as the box was brought to rest. The magnitude of a_2 is less than g. The acceleration graph is shown in Plate II, in which the value of time t increases from right to left, and positive acceleration is registered <u>below</u> the time axis. The tremendous increase in amplitude occurred in the interval of time during which the acceleration decreased to a_2 and

and was maintained at a_2, as described schematically in Figure 6. Attention will be focused on this period. The magnitude of a_2 is near g. Hence a_2 is assumed to be $-g$ in the calculations.

A movie camera took the motion pictures at 250 frames per second. The surface waves had the form and magnitude shown in Plate III when the acceleration was a_2, very shortly after $t = t_2$. The surface form a few milli-seconds after a_2 was reached is shown in Plate IV, from which the tremendous increase in amplitude is very evident indeed.

A more detailed check of the theory was provided by the following procedure. Two values of A were taken from the motion pictures for two values of t very near t_2 but less than t_2. Then from the solution (38), in which, as in (36), α and β can be calculated from the experimental data, B and C are determined. Then the value of A calculated for a value of t less than t_2 is compared with the experimental value. Similarly, with A and dA/dt known at $t = t_2$ (the latter from two values of A at two instants near $t = t_2$), A for $t > t_2$ can be calculated. The values so calculated can be compared with the measured ones. The comparison is shown on Tables 1 to 12. Due to the smallness of A for $t < t_2$, and the consequent difficulty of measurement, the calculated and experimental values of A for $t < t_2$ agreed only in order of magnitude. The agreement between the calculated and experimental values is much better for $t > t_2$. The values of $\sqrt{2}$ given in Tables 1 and 2 are for that in (37) for $t > t_2$.

Both the pictorial description provided by Plates II and III and the more detailed record provided by Tables 1 and 12 demonstrate

very vividly the striking effect of acceleration variation on amplitude increase. The comparison of calculated and experimental values given in these tables also indicates the general validity of the theory given in Sections 3 and 4.

TABLE 1

Max. acceleration = 10.7g	λ = 3.6"		t_2 = 16 millisec.
h = 0.25"	Max. (2A) = 3.19"		$\sqrt{\alpha}$ = 3.06 rad/sec.
t (millisec.)	5	20	25	35
2A Calculated (inches)	0.0015	0.04	0.09	0.19
2A Measured (inches)	0.0010	0.04	0.10	0.22

TABLE 2

Max. acceleration = 10.7g	λ = 3.4"		t_2 = 16 millisec.
h = 0.25"	Max. (2A) = 3.48"		$\sqrt{\alpha}$ = 3.49 rad/sec.
t (millisec.)	5	25	35
2A Calculated (inches)	0.0057	0.12	0.24
2A Measured (inches)	0.0010	0.15	0.25

TABLE 3

Max. acceleration = 12.81g	λ = 3.6"		t_2 = 14 millisec.
h = 0.25"	Max. (2A) = 3.09"		$\sqrt{\alpha}$ = 3.24 rad/sec.
t (millisec.)	5	25	35
2A Calculated (inches)	0.0015	0.12	0.22
2A Measured (inches)	0.0010	0.10	0.20

TABLE 4

Max. acceleration = 12.8g	λ = 3.4"		t_2 = 14 millisec.
h = 0.25"	Max. (2A) = 3.27"		$\sqrt{\alpha}$ = 3.68 rad/sec.
t (millisec.)	5	25	30	35
2A Calculated (inches)	0.006	0.14	0.20	0.26
2A Measured (inches)	0.001	0.12	0.16	0.22

TABLE 5

Max. acceleration = 18.65g	λ = 3.6"		t_2 = 11 millisec.
h = 0.25"	Max. (2A) = 3.16"		$\sqrt{\alpha}$ = 3.16 rad/sec.
t (millisec.)	5	25	40
2A Calculated (inches)	0.012	0.19	0.34
2A Measured (inches)	0.010	0.19	0.30

TABLE 6

Max. acceleration = 18.65g	λ = 3.3"		t_2 = 11 millisec.
h = 0.25"	Max. (2A) = 2.72"		$\sqrt{\alpha}$ = 3.68 rad/sec.
t (millisec.)	5	25	40
2A Calculated (inches)	0.004	0.20	0.45
2A Measured (inches)	0.010	0.18	0.35

TABLE 7

Max. acceleration = 11.65g	λ = 3.4"		t_2 = 14 millisec.
h = 0.5"	Max. (2A) = 1.12"		$\sqrt{\alpha}$ = 4.52 rad/sec.
t (millisec.)	5	40	50
2A Calculated (inches)	0.003	0.14	0.18
2A Measured (inches)	0.001	0.12	0.20

TABLE 8

Max. acceleration = 11.65g	λ = 3.5"		t_2 = 14 millisec.	
h = 0.5"	Max. (2A)= 1.41"		$\sqrt{\alpha}$ = 4.27 rad/sec.	
t (millisec.)	5	25	35	45
2A Calculated (inches)	0.006	0.10	0.18	0.22
2A Measured (inches)	0.008	0.10	0.15	0.20

TABLE 9

Max. acceleration = 13.42g	λ = 3.2"		t_2 = 12 millisec.
h = 0.5"	Max. (2A) = 0.61"		$\sqrt{\alpha}$ = 5.0 rad/sec.
t (millisec.)	5	40	70
2A Calculated (inches)	0.004	0.09	0.18
2A Measured (inches)	0.001	0.10	0.18

TABLE 10

Max. acceleration = 13.42g	λ = 3.4"		t_2 = 12 millisec.
h = 0.5"	Max. (2A) = 1.11"		$\sqrt{\alpha}$ = 4.51 rad/sec.
t (millisec.)	5	20	30	40
2A Calculated (inches)	0.0014	0.05	0.10	0.15
2A Measured (inches)	0.0020	0.04	0.09	0.15

TABLE 11

Max. acceleration = 19.2g	λ = 3.1"		t_2 = 12 millisec.
h = 0.5"	Max. (2A) = 0.57"		$\sqrt{\alpha}$ = 5.3 rad/sec.
t (millisec.)	5	30	40
2A Calculated (inches)	0.0017	0.06	0.09
2A Measured (inches)	0.0020	0.08	0.12

TABLE 12

Max. acceleration = 19.2g	λ = 3.3"		t_2 = 12 millisec.
h = 0.5"	Max. (2A) = 2.34"		$\sqrt{\alpha}$ = 3.43 rad/sec.
t (millisec.)	5	15	25	35
2A Calculated (inches)	0.012	0.05	0.13	0.21
2A Measured (inches)	0.010	0.05	0.11	0.18

7. APPLICATION TO POST-ROLL INSTABILITY OF STOCK ON FOURDRINIER WIRES

The striking effect of acceleration variation on the amplitude of surface disturbances has been demonstrated both theoretically and experimentally. The pertinence of this effect on post-roll instability of stock on a Fourdrinier wire can be seen from the acceleration schedule of the stock as it passes over the table rolls. On top of a table roll the acceleration is downward. Then it increases to a large positive value at a region of reverse curvature which must exist as the wire leaves the roll. As the wire has to become horizontal eventually, the reverse curvature will have to pass over to a region of concave-downward curvature again. This is a region of downward acceleration. Thus the acceleration schedule is much like that given in Figure 5. The latter part of the schedule (Figure 6) is chiefly responsible for the amplitude increase.

One point of great interest is the phase shift of the surface disturbances as they leave the table rolls. A qualitative explanation can be supplied here. For simplicity consider the acceleration schedule described by Figure 3. (The same general conclusion can be reached by considering more complicated and realistic acceleration schedules.) In the region of upward acceleration the solution is given by (28) instead of (27). In (28) s_2 can be very large if a is large, and a large s_2 means a greater frequency and a shorter period of time required for a phase shift of 180°, i.e., for the ridges to become troughs and vice versa.

The growth of surface instability as the stock passes over the table rolls has been adequately explained in Reference 1. In Reference 4 the velocity distribution in the post-roll region was considered a possible cause of an instability of the Taylor-Görtler type, with the presence of growing longitudinal vortex tubes. Although this remains a possibility, the violence of amplitude growth in the post-roll region seems to favor the variability of acceleration as the main cause of instability, particularly since this explanation is entirely independent of the velocity distribution in the post-roll region. The authors believe that the variability of acceleration is indeed the main cause not only of post-roll instability, but also of the instability of the free surface as the stock leaves the slice.

This paper serves as a final report on the research sponsored by TAPPI on free-surface instability for the past several years. The writer of this paper (C.-S. Yih), who has served as supervisor of this research, wishes to express his sincere thanks to TAPPI for this sponsorship, and to the members of the several fluid-mechanics committees of TAPPI, for their interest and many stimulating discussions. The authors also wish to thank Dr. W. R. Debler and Messrs. Milo Kaufman and A. Engerer for assistance in the experimental program.

REFERENCES

1. Yih, C.-S., "Instability of a Rotating Liquid Film with a Free Surface," Proc. Roy. Soc. A, Vol. 258, pp. 63-86, 1960.

2. Yih, C.-S., "Stability of a Rotating Liquid Film," TAPPI, Vol. 45, No. 6, pp. 524-527, 1962.

3. Debler, W. R. and Yih, C.-S., "On the Instability of Stock on a Fourdrinier Wire," TAPPI, Vol. 45, No. 4, pp. 272-279, 1962.

4. Yih, C.-S. and Spengos, A. C., "Free-Surface Instability," TAPPI, Vol. 42, No. 5, pp. 398-403, 1959.

5. Benjamin, T. B. and Ursell, F., "Instability of the Plane Free Surface of a Liquid in Vertical Periodic Motion," Proc. Roy. Soc. A, Vol. 225, pp. 505-515, 1954.

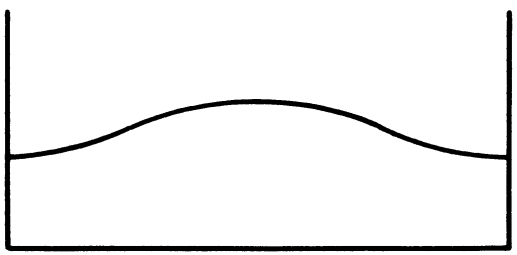

a

$a = a_1$. Wave Attains Maximum Height.

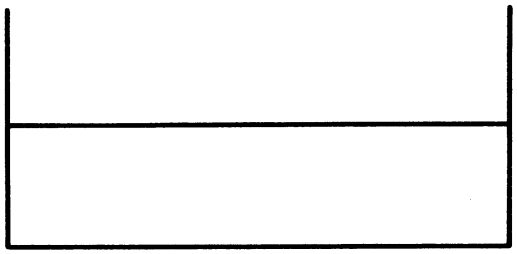

b

a Changes to a_2, Which is Less Than a_1. Surface is Flat.

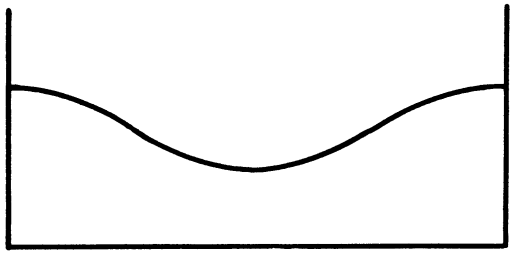

c

$a = a_2$. Wave Attains Next Maximum Height.

Figure 1

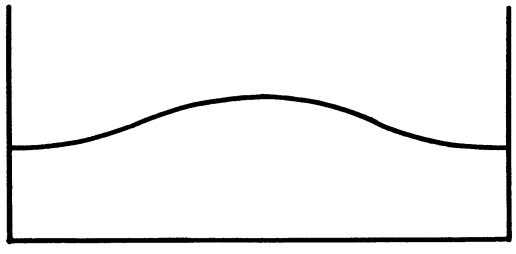

a

$a = a_1$. Wave Attains Maximum Height.

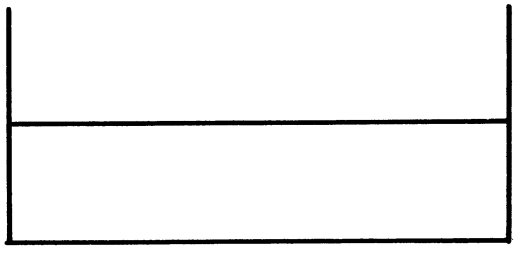

b

a Changes to a_2, Which is Greater Than a_1. Surface is Flat.

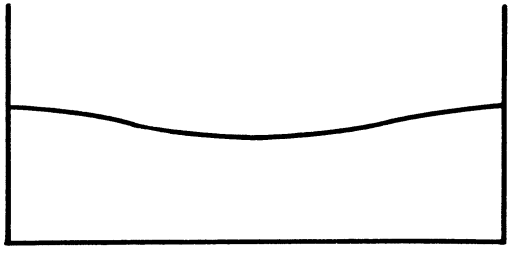

c

$a = a_2$. Wave Attains Next Maximum Height.

Figure 2

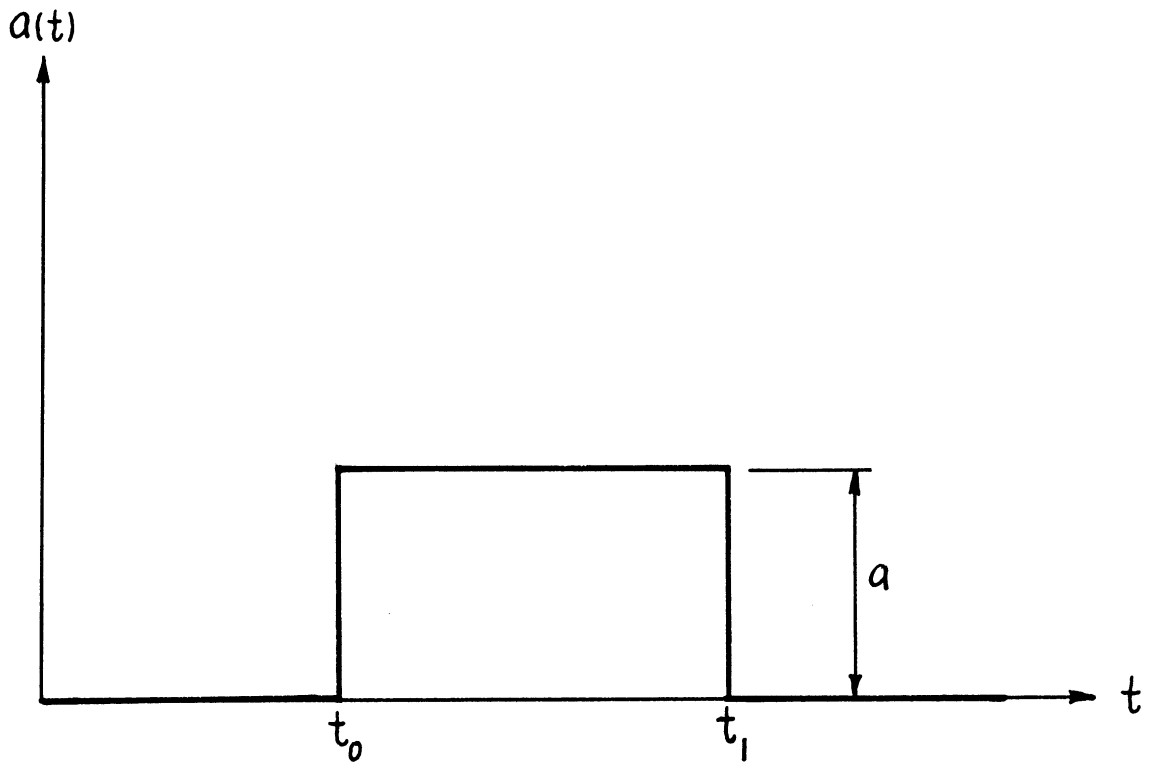

Figure 3. An Idealized Acceleration Schedule.

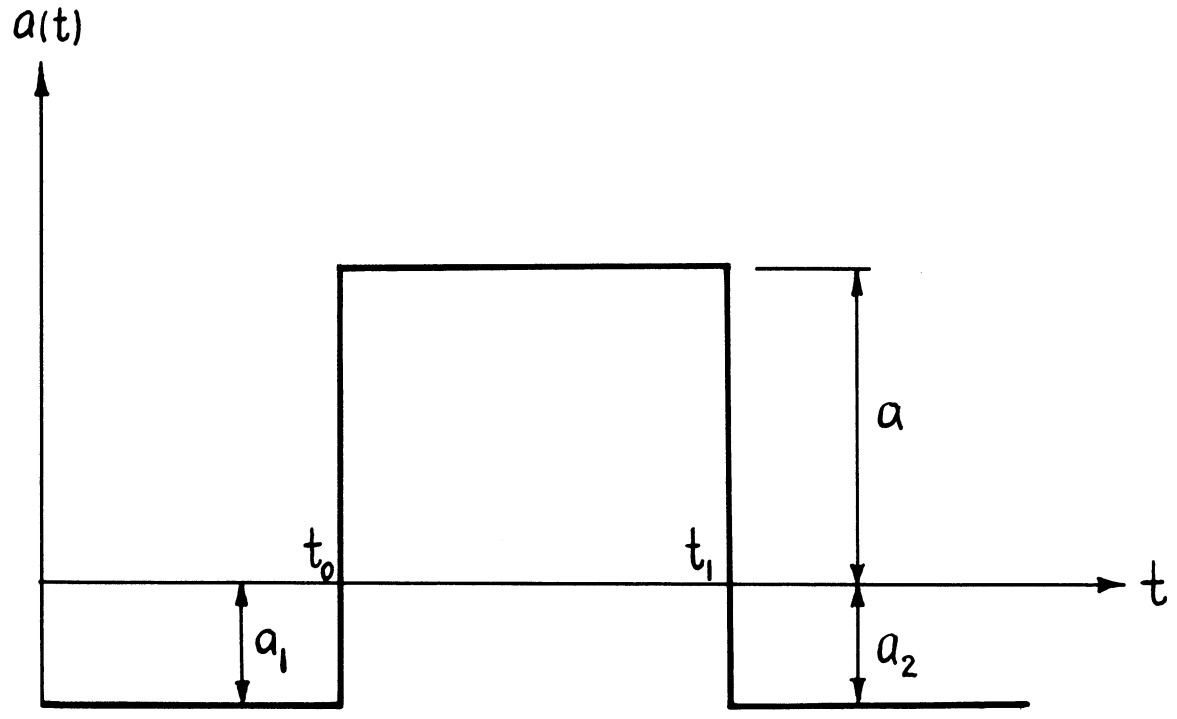

Figure 4. A More Realistic Acceleration Schedule.

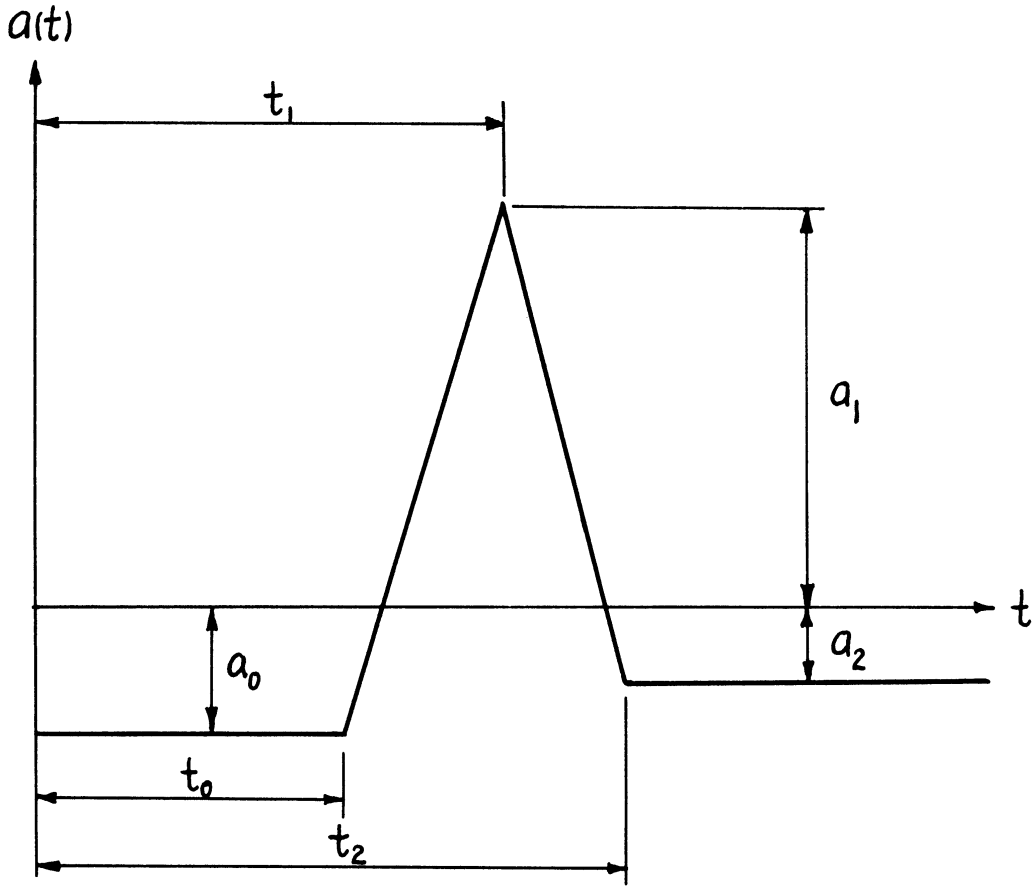

Figure 5. An Acceleration Schedule Representing the Actual Situation on a Fourdrinier Wire.

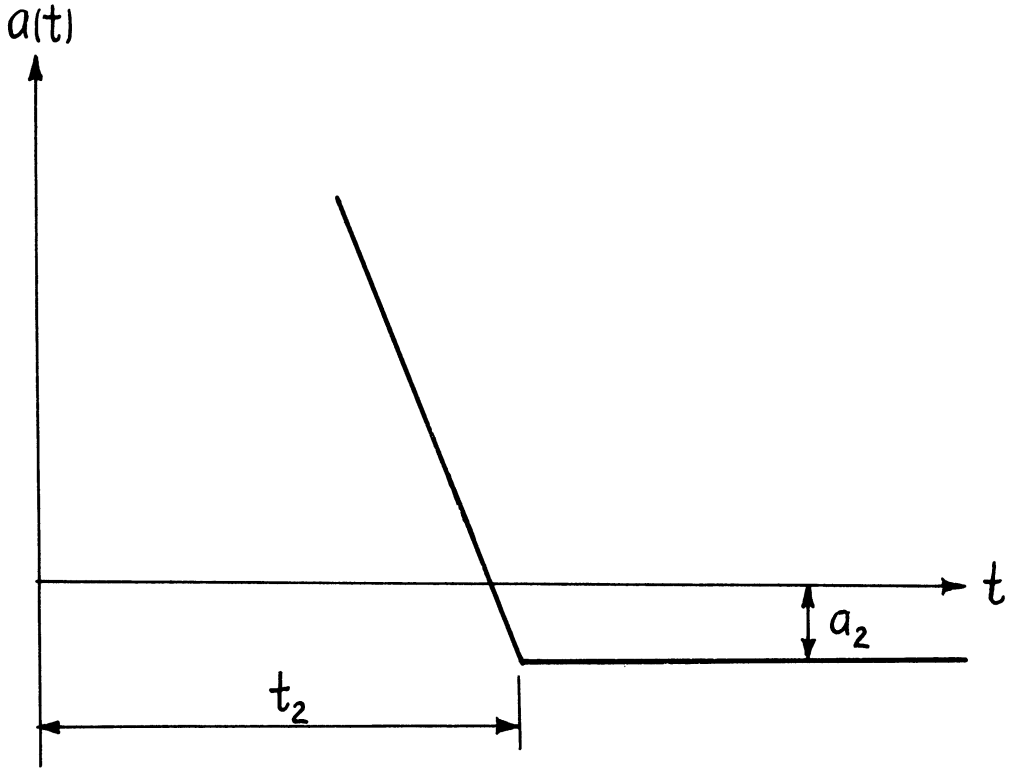

Figure 6. That Portion of Figure 5 Used for Experimental Verification of the Theory.

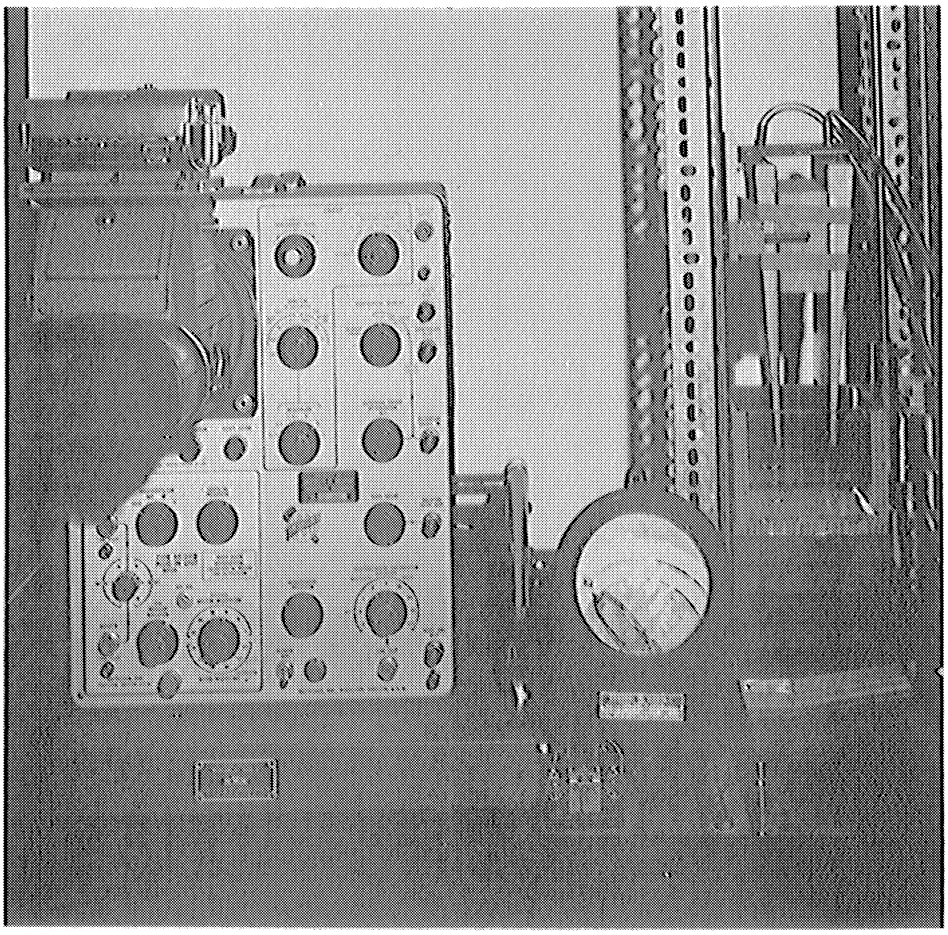

Plate I. Apparatus.

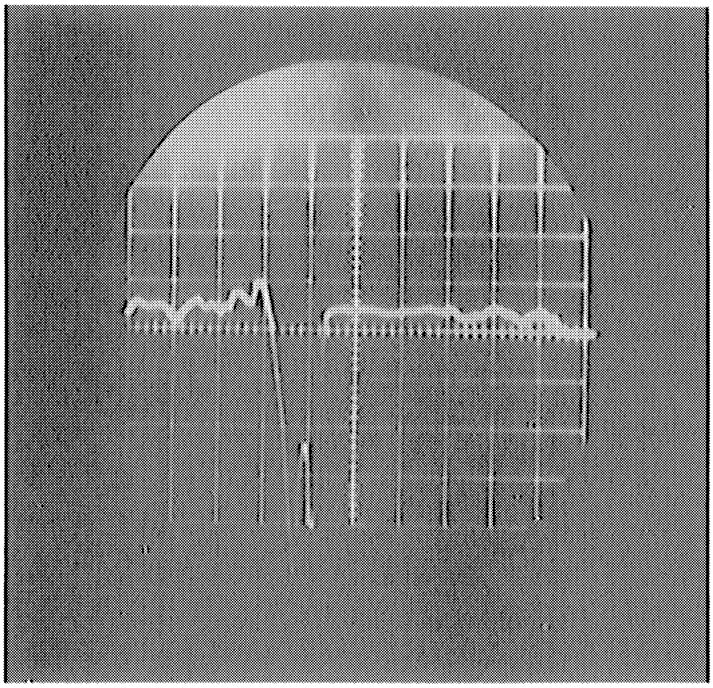

Plate II. Acceleration Graph.

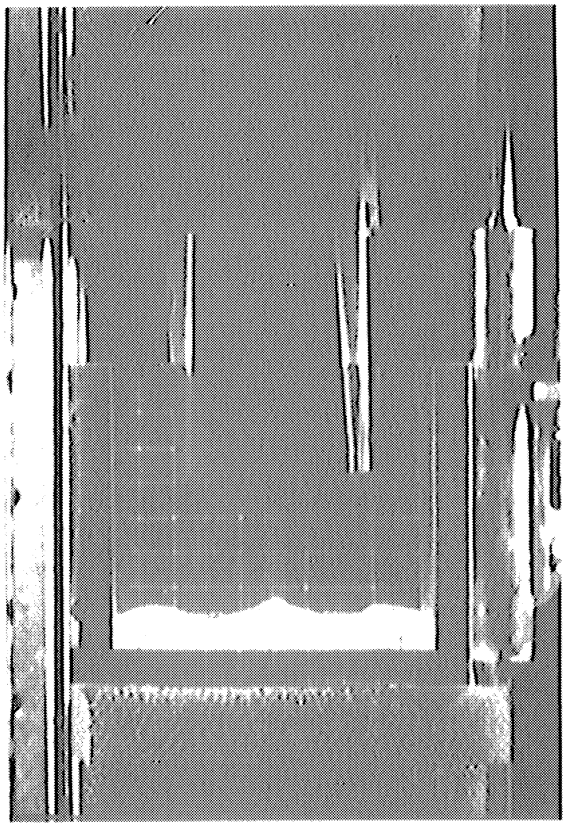

Plate III. Wave Form Soon After a_2 (Nearly Equal to -g) is Reached by a, After Decreasing From a Large Positive Value.

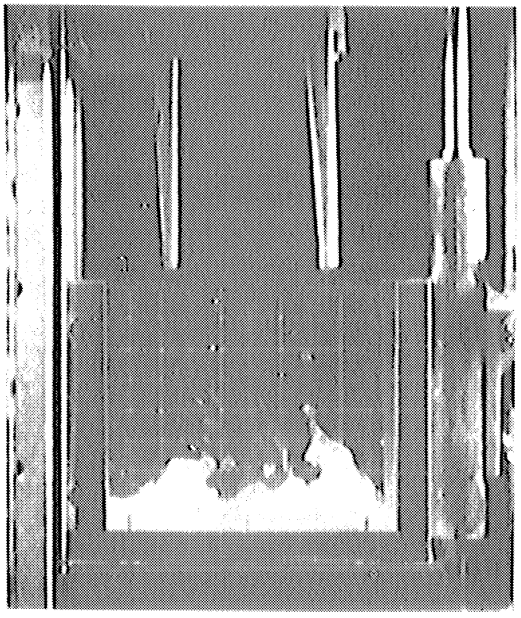

Plate IV. A Few Milli-Seconds After the Condition in Plate III Was Reached.